NASA TECHNICAL NOTE

NASA TN D-4087

ELECTRON FLOW IN LOW-DENSITY ARGON GAS INCLUDING SPACE-CHARGE AND ELASTIC COLLISIONS

by Charles M. Goldstein

Lewis Research Center

Cleveland, Ohio

NATIONAL AERONAUTICS AND SPACE ADMINISTRATION • WASHINGTON, D. C. • JULY 1967

ELECTRON FLOW IN LOW-DENSITY ARGON GAS INCLUDING SPACE-CHARGE AND ELASTIC COLLISIONS

By Charles M. Goldstein

Lewis Research Center
Cleveland, Ohio

NATIONAL AERONAUTICS AND SPACE ADMINISTRATION

For sale by the Clearinghouse for Federal Scientific and Technical Information
Springfield, Virginia 22151 – CFSTI price $3.00

ELECTRON FLOW IN LOW-DENSITY ARGON GAS INCLUDING SPACE-CHARGE AND ELASTIC COLLISIONS*

by Charles M. Goldstein

Lewis Research Center

SUMMARY

The characteristics of one-dimensional electron diode with low-pressure argon scattering gas are analyzed by a Monte Carlo method. Experimentally determined differential elastic scattering cross sections, extrapolated to zero energy, are employed. Current-voltage characteristics are compared with those obtained from a hard-sphere collision model. Negative resistance is found for low emission current densities and low pressure as a result of the Ramsauer cross section. The randomization of energy between velocity components is found to be quite large for accelerating potentials and pressure-electrode separation values as low as 1/2 torr-centimeter. The energy dependence of the total cross section has a much more pronounced effect on the current-voltage curves than the nonisotropic scattering.

INTRODUCTION

A major difficulty in the study of low-density ionized gases is the lack of suitable analytical methods for determining the effects of collisions. "Low density" is here defined as those situations in which a characteristic dimension is of the order of a few mean free paths; that is, the regime wherein neither a collisionless nor a diffusion approximation can be expected to represent the actual situation. This region is of importance in low-pressure thermionic diodes, plasma sheaths, ion engines, and cross-section measurements.

Much effort has been expended to obtain solutions of the Boltzmann transport equation for low-density neutral gases (ref. 1). Little work has been done on the extension of these methods to low-density ionized gases. Sockol (ref. 2) has recently succeeded in numeri-

*Published in J. Appl. Phys., vol. 38, no. 6, June 1967, pp. 2977-2984.

cally integrating the Boltzmann transport equation for a particular low-density ionized gas problem. Unfortunately, the numerical integration proved very difficult for even the simplest hard-sphere collision cross section; the feasibility of using this method for more complex collision cross sections has not as yet been investigated.

The development of a Monte Carlo method for the solution of these problems was discussed in reference 3, and results were presented for the case of a hard-sphere cross section and Lorentz scattering gas. The present paper extends these results to energy and angle dependent scattering cross sections. The particular case treated is that of argon gas, which possesses a Ramsauer total scattering cross section. Argon was chosen as the scattering gas for these studies because of the relative wealth of information concerning the electron-neutral differential cross sections and a reasonably high first excitation potential. The diode characteristics presented herein include current-voltage (I-V) curves, potential and electron-density distributions, and electron velocity and energy-distribution functions.

The Monte Carlo method is, in general terms, a technique for solving physical and mathematical problems by using random sampling. This method has been employed with considerable success to a wide variety of problems, most notably in the area of nuclear shielding problems (neutron transport). A short history of Monte Carlo applications is to be found in the paper by Goertzel and Kalos (ref. 4). An excellent discussion of the basic principles, including applications, is to be found in the recent book by Hammersley and Handscomb (ref. 5), and an extensive bibliography has been compiled by Kraft and Wensrich (ref. 6). While the neutron transport problems are fortunately linear, the method has been extended recently to certain nonlinear radiation transport problems (ref. 7).

There have been some applications of the Monte Carlo method to (1) the kinetic theory of charged particles and (2) the collective interactions between electrons and ions. Papers in the first category (refs. 8 to 10) are concerned with the study of spatially invariant distribution functions in the presence of a uniform electric field; finite geometry and space-charge effects are not considered. Studies in the second category are more properly referred to as "computer experiments." The difference in terminology reflects the fact that these studies approximate the physical model by a finite number of current sheets, which are then followed deterministically through all mutual interactions by the computer. The Monte Carlo method, on the other hand, most frequently implies repeated, stochastically independent trails. A short history of computer experiments is to be found in the paper by Burger (ref. 11). Recently, Burger (ref. 12) has been able to include the effect of a simple collision model and hence demonstrate collisional damping. Computer experiments are not well adapted, however, to the study of steady-state, nonoscillatory solutions employing complex collision cross sections.

FORMULATION OF ELECTRON DIODE PROBLEM

The one-dimensional diode geometry is depicted in figure 1; the electrodes are infinite parallel planes. The electrons are emitted thermionically with a half-Maxwellian velocity distribution:

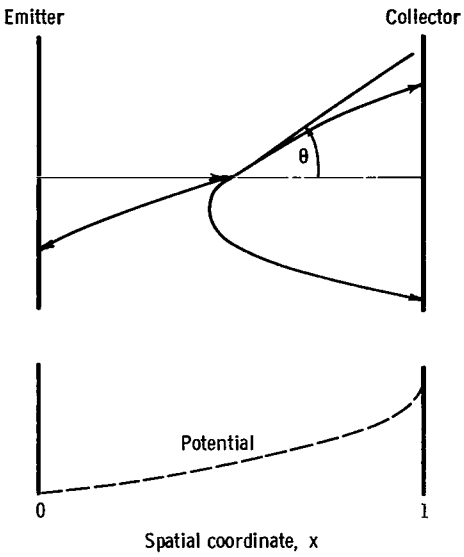

Figure 1. - Diode model and types of scatter.

$$f(u, V) = \frac{4}{\sqrt{\pi}} V e^{-(u^2+V^2)} \qquad \left.\begin{array}{l} 0 \le u \le \infty \\ 0 \le V \le \infty \end{array}\right\} \tag{1}$$

where u is the dimensionless velocity component in the x direction and V is the dimensionless velocity component perpendicular to u. (All symbols are defined in the appendix.) The corresponding dimensional components are given by $u\sqrt{2kT/m}$ and $V\sqrt{2kT/m}$, respectively (m is the electron mass, and kT/e is the emitter temperature in electron volts where e is the electronic charge). Equation (1) is given in cylindrical coordinates with the azimuthal angle integrated out because of the symmetry of the one-dimensional geometry.

The neutral gas is assumed to be stationary and of infinite mass, the electrodes are perfectly absorbing, and the electron density is low enough that only electron-neutral collisions need be considered. Furthermore, the collector potential will be limited to a range wherein electron-neutral interactions are perfectly elastic. This latter restriction implies that the kinetic energy of each electron is a function of only its initial energy and its position x in the diode.

The total and the differential cross sections for elastic electron-neutral scattering in argon have been obtained down to zero energy by employing O'Malley's extrapolation (ref. 13) in conjunction with the experimental data of Ramsauer and Kollath (ref. 14). A plot of the total collision cross section employed and a sketch of the surface obtained by plotting the differential cross section against scattering angle and energy are shown in figure 2. As can be observed in figure 2(b), there is predominant forward scattering at high electron energies.

Our problem is, in essence, to obtain solutions to Poisson's equation

$$\varphi''(x) = Cn(x) \tag{2}$$

where $\varphi = e\tilde{V}/kT$, $\tilde{V}$ is the potential in volts, n(x) is the dimensionless electron density in units of $J_0/e\sqrt{2kT/\pi m}$, J_0 is the emitted electron current density, the space-charge

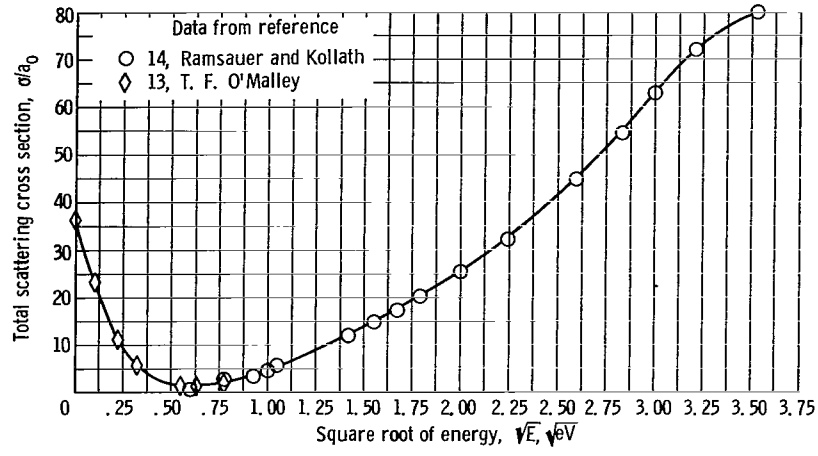

(a) Total scattering.

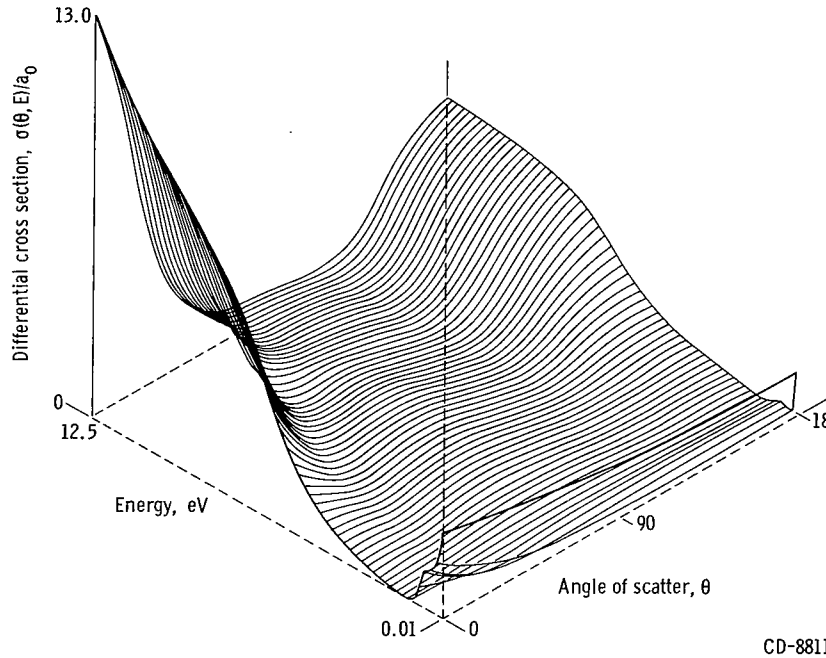

(b) Differential scattering.

Figure 2. - Argon electron cross section.

parameter C is given by

$$C = \left(\frac{8}{\epsilon_0}\right)\left(\frac{\pi}{2kT}\right)^{3/2} m^{1/2} e J_0 L^2, \text{ (mks units)} \tag{3}$$

or

$$C = 4.215\ 10^{11} T^{-3/2} J_0 L^2$$

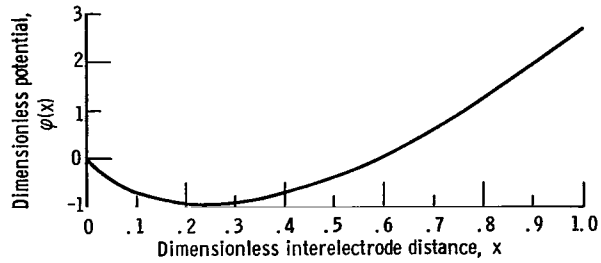

Figure 3. - Potential distribution. Space-charge parameter, C = 50; pressure-distance ratio, pL = 1.0; temperature, T = 1800° K; potential slope, $\varphi'(0) = -10$.

where L is the electrode separation, and the distance from the emitter is given by xL. A typical potential distribution is shown in figure 3.

MONTE CARLO SOLUTION

The general method of solution is discussed in detail in reference 3, hence only a brief summary will be given here.

To initiate a solution of equation (2) for given values of C and $\varphi'(0)$[1], a potential distribution is assumed. The corresponding density distribution is then obtained by sampling a large number of test electrons. It must be emphasized, however, that the initial velocity components of the test "electrons" are not chosen from the distribution function given by equation (1). Test "electrons" is an unfortunate misnomer, since the statistics must be obtained for units of electron flux - not units of charge. Hence, the initial velocities must be chosen from the velocity distribution of flux $g(u, V) \propto uf(u, V)$:

$$g(u, V) = 4uV \exp\left[-(u^2 + V^2)\right] \tag{4}$$

The test electron is then followed throughout its trajectory within the interelectrode space. The distance to collision l_c is chosen from the probability distribution

$$\exp\left(\frac{-l_c}{\bar{\lambda}}\right) \tag{5}$$

where $\bar{\lambda}$ is an effective mean free path. The energy dependent mean free path is obtained from the total collision cross section σ given in figure 2(a) by the expression

[1]The collector potential $\varphi(1)$ was not specified because the Picard iteration employed is not consistently stable under these conditions.

$$\lambda p = \left(\frac{1.01}{\sigma}\right)\left(\frac{T_g}{273}\right) \text{cm-torr} \qquad (6)$$

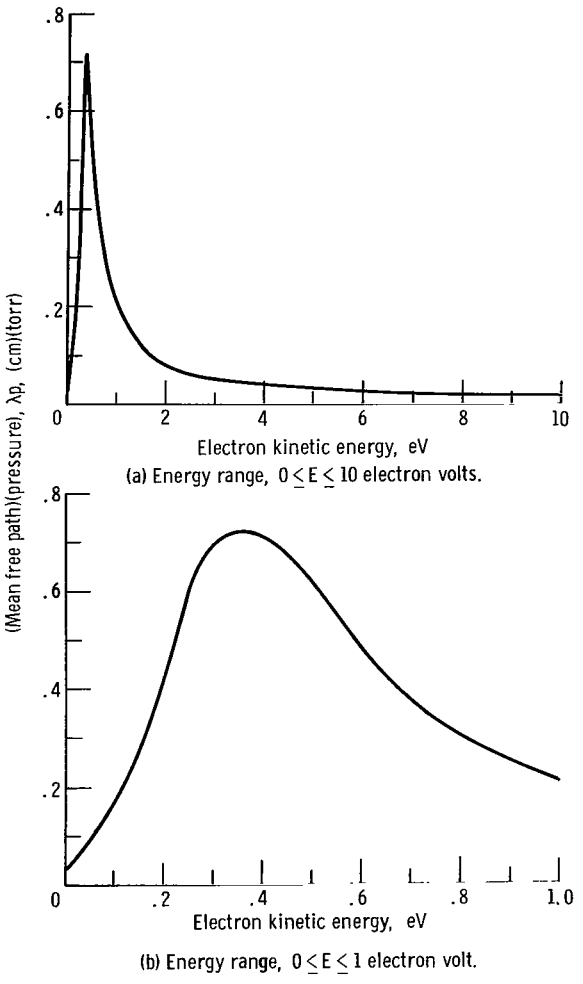

Figure 4. - Argon-electron-atom mean free path; gas temperature, 273° K.

λp is plotted in figure 4 for $T_g = 273^{\circ}$ K, where p and T_g are the gas pressure and temperature, respectively. Now since the mean free path is a function of the electron kinetic energy E (stationary target particles), a $\overline{\lambda}$ is defined in the following way: The interelectrode region is subdivided into a number of cells by imaginary planes parallel to the electrodes. As a test electron enters a cell, the average kinetic energy $\overline{E}$ of the electron in that cell is computed on the assumption that no collision takes place before the electron leaves the cell again. (If the electron does not have a turning point in the cell, then $\overline{E}$ is simply the sum of the kinetic energy entering the cell plus one-half the potential difference across the cell.) The effective mean free path in this cell is then taken to be $\overline{\lambda} \equiv \lambda(\overline{E})$.

The contribution of each test electron to the density n(x) is sampled at prescribed data points x_k. After sampling enough test electrons to obtain reasonable statistics on the sampled quantities $n(x_k)$, a curve fit is effected to obtain n(x). Equation (2) is then solved to obtain a new $\varphi(x)$.

The procedure is continued until convergence on $\varphi(x)$ is obtained (in a statistical sense, ref. 3). The nonlinearity of this problem is evidenced by the fact that n(x) is a function of both collisions and potential.

Each solution of equation (2) results in a potential distribution $\varphi(x)$, a density distribution n(x), and a point on the I-V curve.

RESULTS

In figure 5, current-voltage characteristics are shown for two values of the space-charge parameter C and an emitter temperature of 1800° K (kT = 0.155 eV). The solid

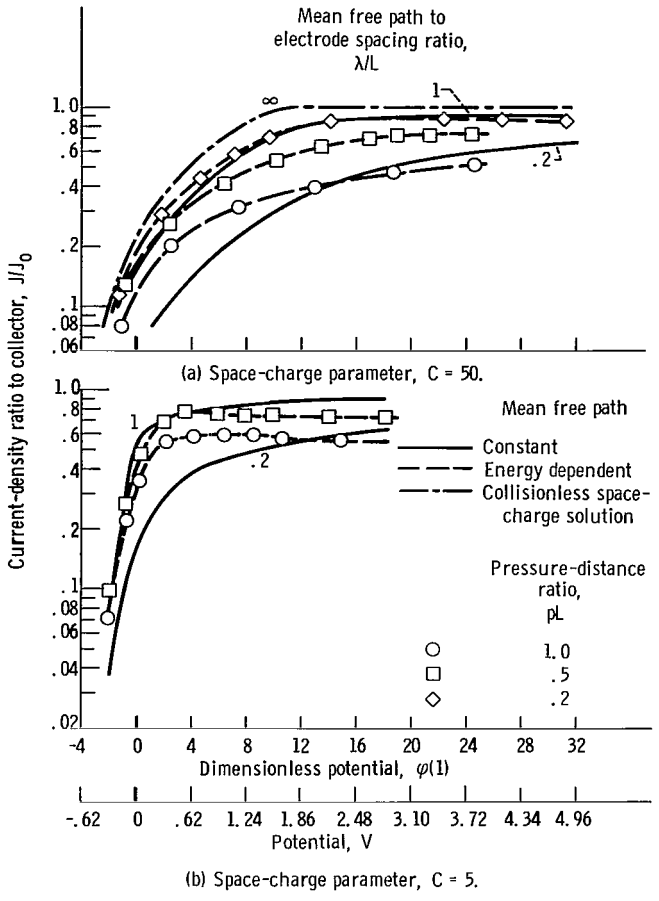

Figure 5. - Effect of mean free path on current-voltage curves. Temperature, T = 1800° K.

curves represent results obtained using energy-independent mean free paths and isotropic scattering. The dot-dash curve was obtained from Langmuirs collisionless space-charge solution (ref. 15). The dashed curves were obtained using argon total and differential scattering cross sections (fig. 2).

Of great interest here is the comparison between the results of the oft employed hard-sphere model (solid curves) and more realistic cross-section data (dashed curves). Consider the lower dashed curve in figure 5(a). Here pL = 1.0. (Note, specifying pL, λ/L is obtained from fig. 4.) For $\varphi(1) \lesssim 0$, this curve lies near the I-V curve for the hard-sphere model corresponding to $\lambda/L = 1$; while for higher collector potentials $\varphi(1) \gtrsim 20$, it lies below the hard-sphere curve $\lambda/L = 0.2$.

In general, the attenuation of current due to collisions is effected in two ways: backscattering collisions which return electrons directly to the emitter and collisions in the interelectrode space which increase the space charge thereby causing more electrons to be reflected by the potential field back to the emitter. The effect of backscattering may be observed in the constant mean free path for high-accelerating potentials (cf. $\lambda/L = 1$ for $\varphi(1) > 18$) where space-charge effects have become negligible.

Both of the above effects can help explain the increased current attenuation at higher potentials for electron flow in argon. For C = 50 (fig. 5(a)), very high potentials must be reached before the space-charge barrier near the emitter is removed $\varphi'(0) = 0$. Until this occurs the collisional attenuation by backscattering is masked by the space-charge effects.

For C = 5 (fig. 5(b)), the situation is different. The space-charge barrier is removed at relatively low collector potentials, and a negative resistance characteristic is observed. The difference in these two cases, C = 50 and C = 5, is illustrated in figures 6(a) and (b). Here potential distributions for $\varphi'(0) = 0$ and $\varphi'(0) = 4$, and the corresponding mean-free-path variations (from fig. 4) for 0.23-electron-volt emitted electrons have

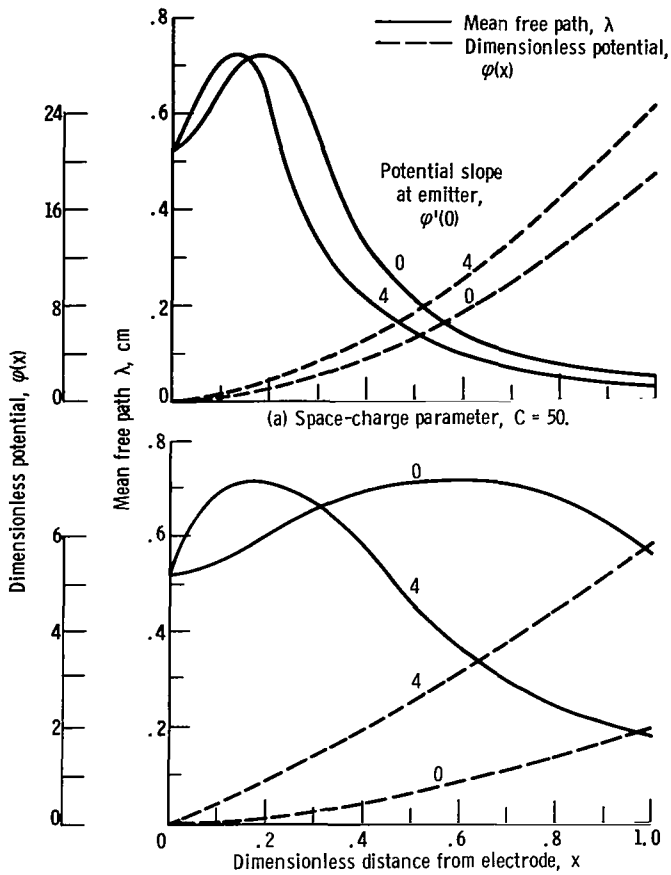

Figure 6. - Effect of space charge on mean free path.

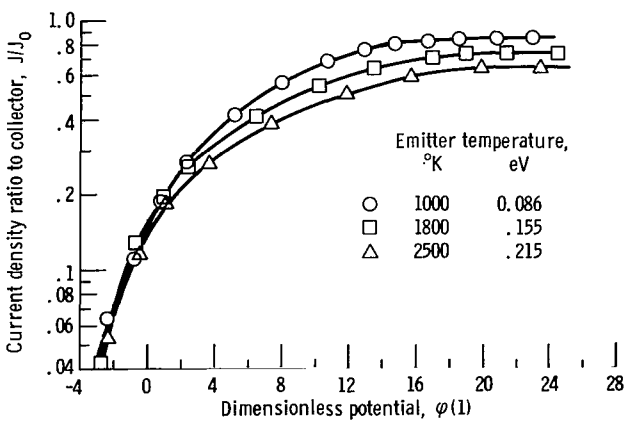

Figure 7. - Effect of emitter temperature on current-voltage curves. Space-charge parameter, C = 50; pressure-distance ratio, pL = 0.5.

been plotted. Note that the area under the mean-free-path curves may be interpreted as the average mean free path across the diode for electrons of this initial energy. After the space-charge barrier is removed $\varphi'(0) = 0$, there is a much more rapid decrease in the average mean free path across the diode for $C = 5$ than for $C = 50$. This decrease results in the observed negative resistance.

In figure 7, the effect of emitter temperature on the I-V curves is shown. For $\varphi(1) = 20$, where $\varphi(1) \equiv \tilde{V}(1)/(kT/e)$, the electrons at the collector are grouped about energies of 1.72, 3.1, and 4.3 electron volts, respectively, in order of increasing emitter temperature. The increased attenuation with temperature is thus most naturally associated with smaller mean free path (see fig. 4). The crossing-over of the upper two curves at lower potentials is no doubt due, once again, to the variation in the mean free path to the left of the maximum in figure 4.

Figure 8 shows the effect of employing the differential collision cross section (dashed curves) rather than assuming isotropic scattering (solid curves). The increase in current for given collector potential obtained when using the differential cross section may be explained on the basis of the predominant forward scattering.

Figure 9 shows a typical set of density distributions for various initial potential slopes. (The corresponding potential distributions for $\varphi'(0) = 0$

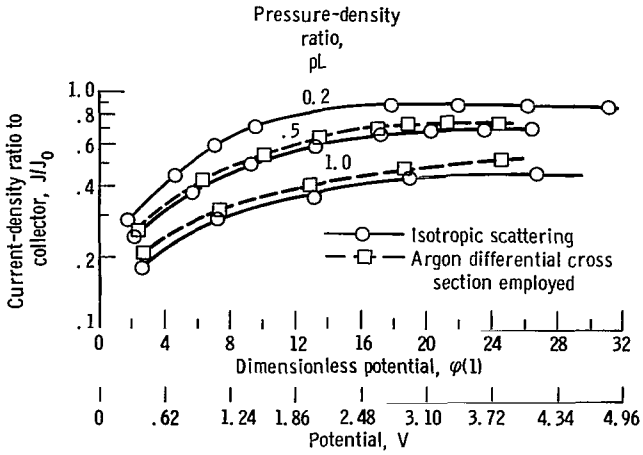

Figure 8. - Effect of nonisotropic scattering on current-voltage curves. Space-charge parameter, C = 50; temperature, T = 1800° K.

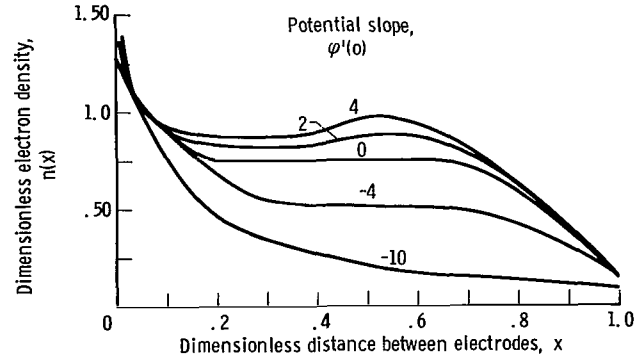

Figure 9. - Electron density distribution. Space-charge parameter, C = 50; temperature, T = 1800° K; pressure-distance ratio, pL = 0.5.

and $\varphi'(0) = 4$ are shown in fig. 6(a)). Of particular interest here is the fact that electron density increases in the inter-electrode region as the collector potential (or, equivalently, $\varphi'(0)$) is increased. This effect is dependent on the cross section and can be explained by reference to figure 6(a). An increase in collector potential ($\varphi'(0)$) causes a decrease in the mean free path away from the emitter. A shorter mean free path implies more collisions which, in turn, cause an increase in the electron density.

DISTRIBUTIONS FUNCTIONS

Until now, only the macroscopic diode characteristics have been discussed. A deeper understanding of diode phenomena is obtained by considering the spatial variation of the velocity and energy distribution functions (hereafter, d.f.) f(u,x) and f(E,x). Note that in the present problem both of these d.f.'s are specified for $x = 0$ and $u > 0$ by equation (1):

$$\left[f(u, 0)\right]_{u>0} = \left(\frac{2}{\sqrt{\pi}}\right) \exp(-u^2) \tag{7}$$

$$\left[f(E, 0)\right]_{u>0} = \left(\frac{2}{\sqrt{\pi}}\right) E^{1/2} \exp(-E) \tag{8}$$

where $E = u^2 + V^2$ is dimensionless energy. To investigate the spatial variation, the d.f.'s were obtained at $x = 0$, $1/2$, and 1 by sampling a large number of electrons (4000) for the two following cases:

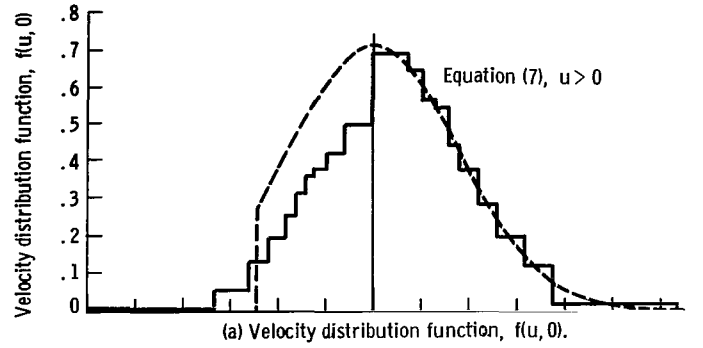

(a) Velocity distribution function, f(u, 0).

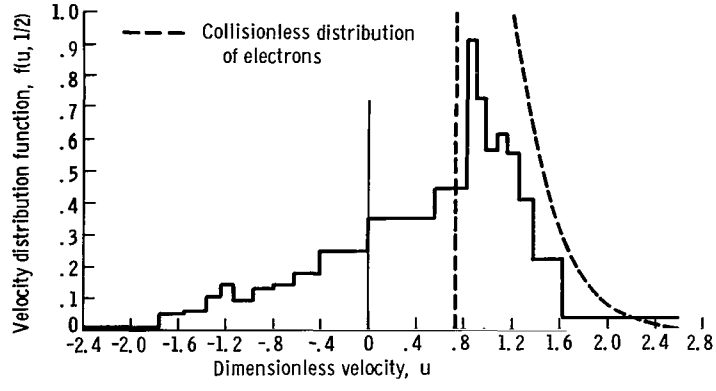

(b) Velocity distribution function, f(u, 1/2); potential, $\varphi(1/2) = -0.4$.

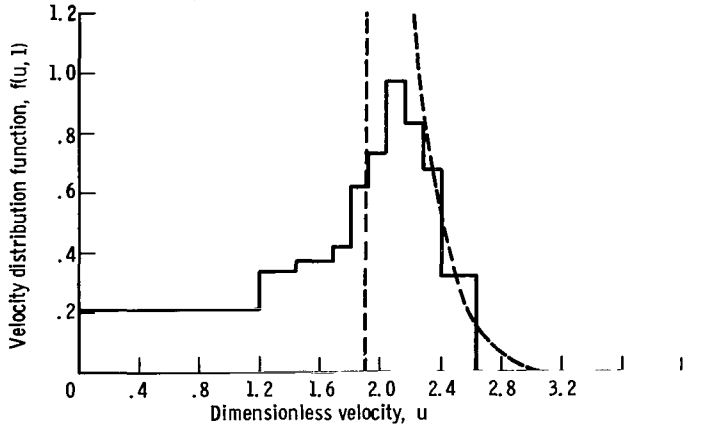

(c) Velocity distribution function, f(u, 1); potential, $\varphi(1) = 2.68$.

Figure 10. - Variation in velocity distribution function. Space-charge parameter, C = 50; pressure-distance ratio, pL = 1; temperature, T = 1800° K; potential slope, $\varphi'(0) = -10$; potential minimum, $\varphi_m = -0.94$; location of potential minimum, $x_m = 0.23$.

Case 1: Space-Charge Barrier

The distribution functions shown in figures 10 and 11 correspond to the potential distribution shown in figure 3 (p. 5) and the density distribution shown in figure 9 for $\varphi'(0) = -10$.

The sampled d.f., or histogram, for the u-component of velocity is shown in figures 10(a), (b), and (c), for $x = 0$, $1/2$, and 1, respectively. Equation (7) is also shown in figure 10(a) for comparison. In the case of no collisions, all electrons emitted with $u^2 < -\varphi_m$ would be returned to the emitter by the space-charge barrier; the d.f. of these electrons is shown as a dashed line in figure 10(a) where $u < 0$. The deviation between this curve and the histogram for $u < 0$ is caused by collisions. Even though the density of electrons for $0 > u > -0.94$ has been reduced, calculations show that the current (or flux) of electrons back to the emitter is increased.

In figure 10(b), the u-component d.f. at the half-way position $x = 1/2$ in the diode is shown. Since this position is to the right of the potential minimum (cf. fig. 3), there would be a null electron population for $u < \sqrt{-\varphi(1/2)} = \sqrt{0.425}$ in the collisionless case.

The d.f. $f(u, 1)$ is shown in figure 10(c). Here, there are no electrons with $u < 0$ since the collector (and emitter) has been assumed to be perfectly absorbing. The collisionless d.f. is also shown by the dashed curve. Comparison with the collisionless distribution shows that collisions have greatly reduced the population of electrons with large values of u. In other words, a portion of the x-directed energy acquired from the electric field has been randomized by collisions.

The energy d.f.'s, $f(E, 0)$ and $f(E, 1)$, are shown in figure 11. The slight deviation between the histogram of $f(E, 0)$ and equation (8) (shown dashed) is caused by the electrons returned to the emitter by collisions and reflection from the space-charge barrier. The depletion of low-energy electrons by collisions is vividly portrayed by comparison with the collisionless d.f. (dashed curve, fig. 11) at the collector. Since all collisions treated here are perfectly elastic, the only effect that can cause a difference between these curves is this depletion.

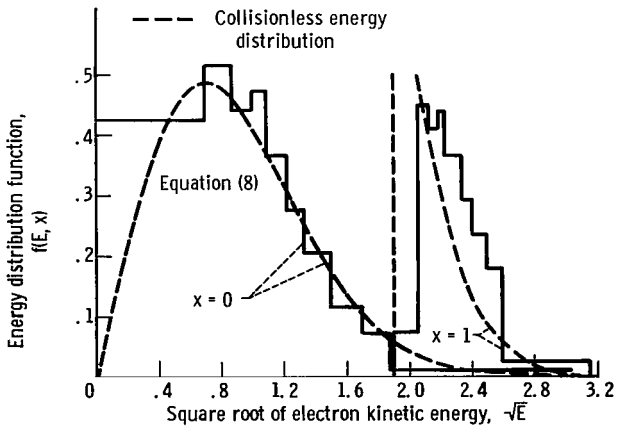

Figure 11. - Effect of energy distribution function on square root of electron kinetic energy. Space-charge parameter, $C = 50$; pressure-distance ratio, $pL = 1$; potential slope, $\varphi'(0) = -10$; collector potential, $\varphi(1) = 2.68$; potential minimum, $\varphi_m = -0.94$.

Case 2: Monotonic Accelerating Potential

In figures 12 and 13 the velocity and energy d.f.'s are shown corresponding to the potential distribution shown in fig-

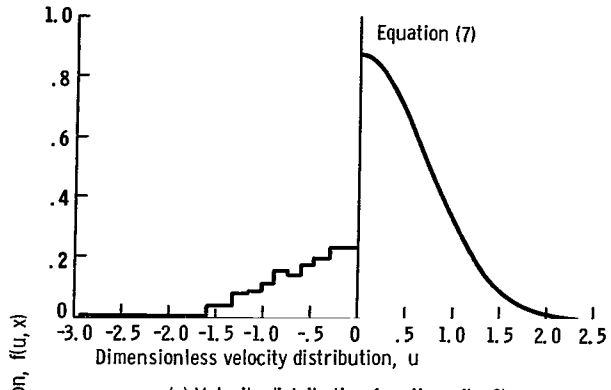

(a) Velocity distribution function, f(u, 0).

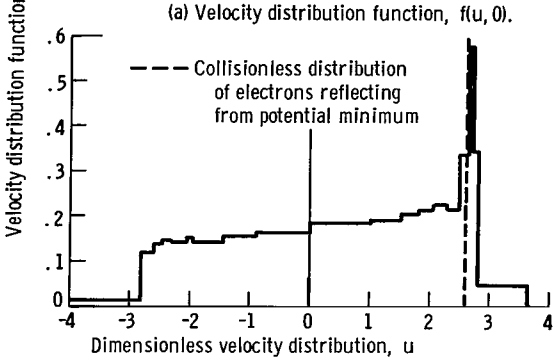

(b) Velocity distribution function, f(u, 1/2); dimensionless potential, $\varphi(1/2) = 6.76$.

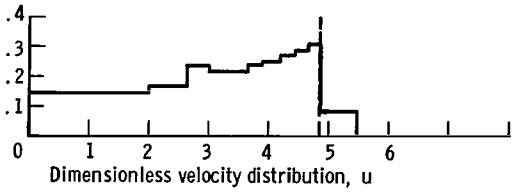

(c) Velocity distribution function, f(u, 1); dimensionless potential, $\varphi(1) = 23.57$ (3.65 electron volts).

Figure 12. - Variation in velocity distribution function. Space-charge parameter, C = 50; pressure-distance ratio, pL = 0.5; temperature, T = 1800° K; potential slope, $\varphi'(0) = 4$.

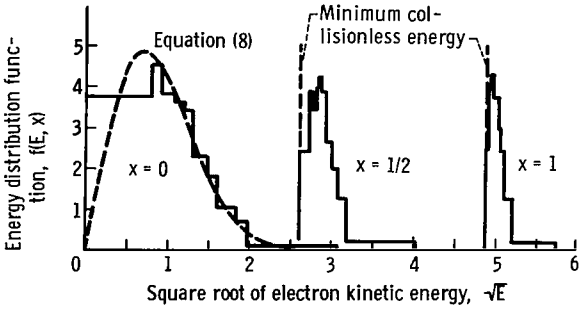

Figure 13. - Variation in energy distribution function.

ure 6(a) for $\varphi'(0) = 4$. In contrast to the previous case, no space-charge barrier is present here; also, the average mean free path through the diode (see figs. 6 and the discussion thereof) is less, and hence, the collisional activity is much greater.

Figure 12(a) shows relatively little backscattering to the emitter ($u < 0$). A large mean free path near the emitter (fig. 6(a)) accounts for this. Backscattered electrons further from the emitter have a greater probability of being reflected by the potential field.

The peak in f(u, 1/2) (fig. 12(b)) is caused by the population of electrons that have not undergone collisions. The still greater collisional activity near the collector all but wipes out this peak (fig. 12(c)). These curves are in distinct contrast to those of Case 1 (figs. 10(b) and (c)).

Comparing figure 13 with figure 11 shows the effect of lesser depletion of the electrons at the emitter on the energy d.f.

Reliability of the Monte Carlo Calculations

At the present time, no rigorous method exists of evaluating the accuracy of the Monte Carlo calculations presented in this report. At best, certain limiting cases are amenable to analytical solution, and hence, may be used as a check on the methodology. One such limiting case is that of a hard-sphere, single-collision model (ref. 16). The Monte Carlo program (ref. 17) employed for the present calculations was checked against this model, and agreement was obtained within

three significant figures on evaluations of diode current for given collector potentials.

Sockol (ref. 2) pointed out a peculiar deviation between his results and the Monte Carlo results of reference 3, however. Although the I-V curves resulting from both methods were in excellent agreement, the correlation between points on the curves corresponding to the same initial condition ($\varphi'(0)$) was bad, especially at low collector potentials. This discrepancy has been clarified and is caused by a peculiar insensitivity of the ordered pairs ($\varphi(1)$, J/J_o) defining the I-V curve to the initial conditions $\varphi'(0)$. This can be observed in table I where the underlined values represent the boundary condition specified (in addition to $\varphi(0) = 0$). Computed values are shown with the computed standard deviation (10 trials). Although the variation in $\varphi'(0)$ is large, the currents corresponding to the same collector potentials show excellent agreement.

TABLE I. - VARIATION OF $\varphi(0)$ AND $\varphi(1)$

Potential slope at x = 0, $\varphi'(0)$	Potential at x = 1, $\varphi(1)$	Current density ratio, J/J_o
-12	-0.822±0.12	0.115±0.005
-12.27±0.36	-.822	.116± .007
-11.73± .30	-.17	.145± .008
[a]-12	[a]-.17	[a].143

[a]Ref. 2.

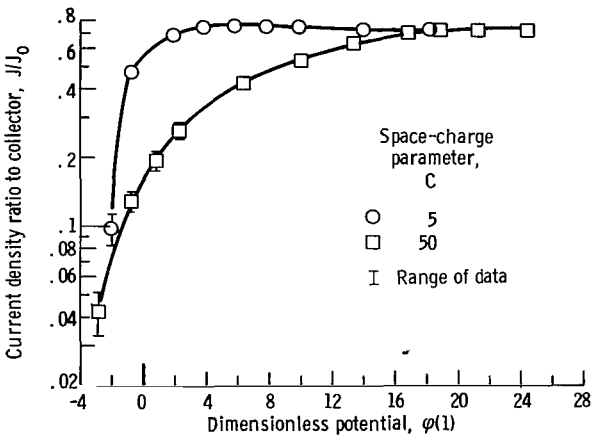

Figure 14. - Reliability of computed values. Temperature, 1800° K, pressure-distance ratio, pL = 0.5.

The points on the I-V curves of figure 5 (p. 7) were obtained by averaging the currents and the collector potentials obtained from 10 iterations. The standard deviation of current σ_J and voltage σ_φ were also computed for each point from the 10 samples. For C = 50, the average standard deviations so computed were $\sigma_J \approx 0.006$ and $\sigma_\varphi \approx 0.26$, while for C = 5, $\sigma_J \approx 0.006$ and $\sigma_\varphi \approx 0.023$. In figure 14, the data points are plotted for two cases, and the ranges of $\pm 2\sigma$ are explicitly indicated wherever they extend beyond the symbols employed. As can be observed, the characteristics of the curves are unambiguous.

CONCLUSION

The electron flow through argon gas has been analyzed for different space-charge conditions by a Monte Carlo method. The electrode spacings and pressures investigated are such that the velocity distribution functions do not reach a spatially constant form.

In comparing a hard-sphere collision model with the more realistic model, it is ob-

served that the energy dependence of the total cross section has a much more noticeable effect on the current-voltage curves than the nonisotropic scattering. At weaker space-charge conditions, the energy dependence of the total cross section even results in a negative resistance characteristic.

The velocity distributions show considerable randomization between velocity components (parallel and perpendicular to the applied field). The energy distributions demonstrate the effect of electrons returned to the emitter, for those electrons reaching the collector after undergoing only elastic collision will have the same velocity and energy distribution functions there as they would have with no collisions. Hence, the difference between the derived energy histograms at the collector and the collisionless velocity and energy distribution functions is due entirely to the electrons returned to the emitter. As would be expected from consideration of the energy-dependent mean free path, there is a predominant depletion of low-energy electrons.

The results herein obtained from consideration of the best available elastic scattering cross sections are such as to defy accurate prediction, even in a qualitative sense. Yet, once obtained, they are relatively easy to explain. Therein lies perhaps the greatest value of the Monte Carlo method. Although it has certain drawbacks, such as quantitative inaccuracies and/or stringent computer requirements, no other method exists to date for the study of these problems. It is hoped that the insight gained by these studies will eventually lead to the development of still more powerful methods.

Lewis Research Center,
National Aeronautics and Space Administration,
Cleveland, Ohio, October 13, 1966,
129-02-01-05.

APPENDIX - SYMBOLS

a_o	Bohr cross section
C	space-charge parameter
E	dimensionless electron kinetic energy
f(E,x)	energy distribution function
f(u,x)	velocity distribution function
J/J_o	current-density ratio to collector
J_o	emitted electron current density
kT	emitter temperature, eV
L	electrode separation
l_c	distance for collision
m	electron mass
n(x)	dimensionless electron density
p	gas pressure
T_g	gas temperature
u	dimensionless velocity component in x-direction
V	dimensionless velocity component transverse to u
x	dimensionless distance from emitter
λ	mean free path
$\bar{\lambda}$	effective mean free path
σ	total collision cross section
σ_J	standard deviation of current to collector
σ_φ	standard deviation of collector potential
φ_m	potential minimum
$\varphi(x)$	dimensionless potential
$\varphi(1)$	collector potential
$\varphi'(0)$	potential slope at emitter

REFERENCES

1. Grad, H.: Theory of Rarefied Gases. Proceedings of the 1st International Symposium on Rarefied Gas Dynamics, Fernand M. Devienne, ed., Pergamon Press, 1959, pp. 100-138.

2. Sockol, Peter M.: Flow of Electrons Through a Rarefied Gas Between Plane Parallel Electrodes. NASA TN D 3510, 1966.

3. Goldstein, Charles M.: Monte Carlo Method for the Calculation of Transport Properties in a Low-Density Ionized Gas. TN D-2959, 1965.

4. Goertzel, Gerald; and Kalos, Melvin H.: Monte Carlo Method in Transport Problems. Physics and Mathematics. Vol. 2 of Progress in Nuclear Energy, Series 1, D. J. Hughes, J. E. Sanders, and J. Horowitz, eds., Pergamon Press, 1958, pp. 315-369.

5. Hammersley, J. M.; and Handscomb, D. C.: Monte Carlo Methods. John Wiley and Sons, Inc., 1964.

6. Kraft, Rose; and Wensrich, Carl J.: Monte Carlo Methods: A Bibliography Covering the Period 1949 to 1963. Rept. No. UCRL-7823, University of California, Lawrence Radiation Lab., Apr. 1, 1964.

7. Fleck, J. A., Jr.: The Calculation of Nonlinear Radiation Transport by a Monte Carlo Method. Methods in Computational Physics. Vol. 1. B. Alder, ed., Academic Press, 1963, pp. 43-65.

8. Itoh, T.; and Musha, R.: Monte Carlo Calculations of the Motions of Electrons in Helium. J. Appl. Phys., vol. 31, no. 4, Apr. 1960, pp. 744-745.

9. Yarnold, G. D.: The Energies of Uniformly Accelerated Particles in a Gas. Phil. Mag., vol. 36, no. 254, Mar. 1945, pp. 185-200.

10. Wannier, G. H.: Motion of Gaseous Ions in Strong Electric Fields. Bell Syst. Tech. J., vol. 32, no. 1, Jan. 1953, pp. 170-254.

11. Burger, P.: The Opposite-Stream Plasma Diode. Rept. No. SEL-64-012 (NASA CR-58200), Stanford University, Electronics Lab., Apr. 1964, p. 41.

12. Burger, Peter: Computer Simulation Methods for Plasma Diodes With Collisions. Proceedings of the Thermionic Conversion Specialist Conference, 1965, pp. 65-68.

13. O'Malley, Thomas F.: Extrapolation of Electron-Rare Gas Atom Cross Sections to Zero Energy. Phys. Rev., vol. 130, no. 3, May 1, 1963, pp. 1020-1029.

14. Ramsauer, C.; and Kollath, R.: Die Winkelveiterlung bei der Streuung langsamer Electronen an Gas molekuelen, III. Ann. Physik, vol. 12, 1932, pp. 837-848.

15. Langmuir, Irving: The Effect of Space Charge and Initial Velocities on the Potential Distribution and Thermionic Current Between Parallel Plane Electrodes. Phys. Rev., vol. 21, Apr. 1923, pp. 419-435.

16. Goldstein, Charles M.; and Goldstein, Arthur W.: A Single-Collision Model for Electron-Beam Currents Between Plane Electrodes. NASA TN D-3058, 1965.

17. Swigert, Paul; and Goldstein, Charles M.: Monte Carlo Code for Solution of Planar Electron-Diode Problems Including Electron-Neutral Elastic Collisions. NASA TN D-4043, 1967.

NASA-Langley, 1967 —— 25 E-3621

"The aeronautical and space activities of the United States shall be conducted so as to contribute . . . to the expansion of human knowledge of phenomena in the atmosphere and space. The Administration shall provide for the widest practicable and appropriate dissemination of information concerning its activities and the results thereof."

—NATIONAL AERONAUTICS AND SPACE ACT OF 1958

NASA SCIENTIFIC AND TECHNICAL PUBLICATIONS

TECHNICAL REPORTS: Scientific and technical information considered important, complete, and a lasting contribution to existing knowledge.

TECHNICAL NOTES: Information less broad in scope but nevertheless of importance as a contribution to existing knowledge.

TECHNICAL MEMORANDUMS: Information receiving limited distribution because of preliminary data, security classification, or other reasons.

CONTRACTOR REPORTS: Scientific and technical information generated under a NASA contract or grant and considered an important contribution to existing knowledge.

TECHNICAL TRANSLATIONS: Information published in a foreign language considered to merit NASA distribution in English.

SPECIAL PUBLICATIONS: Information derived from or of value to NASA activities. Publications include conference proceedings, monographs, data compilations, handbooks, sourcebooks, and special bibliographies.

TECHNOLOGY UTILIZATION PUBLICATIONS: Information on technology used by NASA that may be of particular interest in commercial and other non-aerospace applications. Publications include Tech Briefs, Technology Utilization Reports and Notes, and Technology Surveys.

Details on the availability of these publications may be obtained from:

SCIENTIFIC AND TECHNICAL INFORMATION DIVISION

NATIONAL AERONAUTICS AND SPACE ADMINISTRATION

Washington, D.C. 20546